

Are the Light-harvesting I Complexes from *Rhodospirillum rubrum* Arranged Around the Reaction Centre in a Square Geometry?

Henning Stahlberg^{1,2}, Jacques Dubochet¹, Horst Vogel²
and Robin Ghosh^{3*}

¹Laboratory for Ultrastructural Research (LAU), Biology Department, University of Lausanne (UNIL), CH-1015 Lausanne, Switzerland

²Laboratory of Physical Chemistry of Polymers and Membranes (LCPPM) Chemistry Department, Swiss Federal Institute of Technology (EPFL), CH-1015 Lausanne Switzerland

³Laboratory of Bioenergetics University of Geneva Ch. des Embouchis, CH-1254 Jussy-Lullier, Switzerland

The basic photosynthetic unit containing the reaction centre and the light-harvesting I complex (RC-LHI) of the purple non-sulphur bacterium *Rhodospirillum rubrum* was purified and reconstituted into two-dimensional (2D) membrane crystals. Transmission electron microscopy using conventional techniques and cryoelectron microscopy of the purified single particles and of 2D crystals yielded a projection of the RC-LHI complex at a resolution of at least 1.6 nm. In this projection the LHI ring appears to have a square symmetry and packs in a square crystal lattice. The square geometry of the LHI ring was observed also in images of single isolated particles of the RC-LHI complex. However, although the LHI units are packed identically within the crystal lattice, a new rotational analysis developed here showed that the reaction centres take up one of four possible orientations within the ring. This fourfold disorder supports our interpretation of a square ring symmetry and suggests that a hitherto undetected component may be present within the photosynthetic unit.

© 1998 Academic Press

Keywords: light-harvesting I complex; reaction centre; *Rhodospirillum rubrum*; transmission electron microscopy; image processing

*Corresponding author

Introduction

In recent years, the structural organisation of the photosynthetic membrane from purple sulphur and non-sulphur bacteria has come under increasingly close scrutiny. The majority of purple bacteria contain at least two light-harvesting complexes, designated light-harvesting complex I

(LHI) and light-harvesting complex II (LHII), which can collect and transfer light energy to a reaction centre (RC) in a highly efficient manner. The reaction centre is able to utilise light energy to perform the primary steps of photosynthesis, charge separation, which ultimately leads to the generation of chemical energy (for reviews, see Deisenhofer & Michel, 1989; Drews, 1985).

LHI and LHII are able to absorb light throughout the visible to near-infrared (near-IR) region and transfer energy to the near-IR absorption maximum of the associated pigment, bacteriochlorophyll a (BChla) at 880 nm and 800 to 850 nm, respectively. The spectral overlap of the near-IR absorption maxima with each other and with the bacteriochlorophyll special pair of the reaction centre (P870) ensures that energy is primarily transferred in the sequence LHII-to-LHI-to-RC.

The molecular details of these individual complexes are now being elucidated in detail. The structure of the reaction centres for *Rhodospseudomonas viridis* (Deisenhofer *et al.*, 1985) and *Rhodobacter sphaeroides* (Allen *et al.*, 1987) have been solved and recently the structure of the LHII complex from

This paper is dedicated to Prof. Wolfhart Rüdiger on the occasion of his 65th birthday.

Present address: R. Ghosh, Department of Bioenergetics, Institute of Biology, University of Stuttgart, D-70550 Stuttgart, Germany.

Abbreviations used: 2D, two-dimensional; β OF, β -octylglucoside; BChla, bacteriochlorophyll a; DEAE, diethylaminoethyl; DHPC, diheptanoyl-*sn*-phosphatidylcholine; DOPC, dioleoyl-*sn*-phosphatidylcholine; IR/VIS, infrared and visible light; LHI, light-harvesting complex I; L:P, lipid-to-protein ratio; RC, reaction centre; RC-LHI, reaction centre associated with the light-harvesting complex I; TEM, transmission electron microscopy.

E-mail address of the corresponding author: Robin.Ghosh@po.uni-stuttgart.de

Rhodospseudomonas acidophila (McDermott *et al.*, 1995) and *Rhodospirillum molischianum* (Koepeke *et al.*, 1996) have been solved at atomic resolution by X-ray crystallography, and a projection map at 0.85 nm resolution of the LHI complex from *Rhodospirillum rubrum* has been obtained by cryoelectron microscopy of two-dimensional crystals (Karrasch *et al.*, 1995). All of these data confirm early biochemical experiments (see Zuber, 1985) indicating that the complexes contain two non-identical polypeptides, α and β , which bind BChla and carotenoid. In addition, as might be expected from the relatively high level of sequence homology between α and β polypeptides for different complexes, the three-dimensional structures of LHII and the projection map from LHI reveal a similar arrangement of polypeptides and pigments. Thus the LHII complexes from *Rps. acidophila* and *R. molischianum* are composed of nine and eight dimers, respectively, each binding three BChla molecules and one or two molecules of carotenoid, and arranged in a ring-like structure within the plane of the membrane. For the LHI from *R. rubrum*, even the lower-resolution projection map is sufficient to reveal that 16 $\alpha\beta$ dimers are arranged in a ring within the plane of the membrane with the 32 transmembrane α -helices fixed in an orientation similar to those observed for the LHII complexes (Karrasch *et al.*, 1995).

An important question concerns the interaction of the reaction centre with the LHI ring. Although early low-resolution electron microscopic analyses of naturally occurring 2D RC-LHI crystals suggested a single reaction centre to be present within a ring of LHI complexes (Miller, 1982; Engelhardt *et al.*, 1986), kinetic studies (Joliot *et al.*, 1990) employing isolated chromatophores implied that two reaction centres were interacting with the LHI complexes. However, Karrasch *et al.* (1995) were able to fit only a single reaction centre within the LHI ring projection as obtained using cryoelectron microscopic data, supporting the conclusions of later kinetic studies (Fernández-Velasco & Crofts, 1991) that were in conflict with those of Joliot *et al.* (1990). Recently, Walz & Ghosh (1997) obtained 2D crystals from the RC-LHI complex similar to those described here and were able to show that the LHI rings from a carotenoid-less mutant do indeed accommodate one RC. In this latter study, the RC-LHI complexes were obtained intact by gentle dissociation of the native membranes prior to crystallisation. This detergent procedure did not cause dissociation of the LHI complexes to the small soluble subunits characterised by an absorption maximum at 820 nm (B820: Miller *et al.*, 1987; Ghosh *et al.*, 1988a,b) thus strengthening the conclusion that the structural data observed correspond to the *in vivo* situation. However, the micrographs obtained from negatively stained RC-LHI complexes by Walz & Ghosh (1997) were processed by direct cross-correlational averaging and, although the LHI projection strongly resembled that obtained by

cryoelectron microscopy, the reaction centre could be visualised only as a featureless object within the LHI ring. It was suggested that the lack of features was due to rotational disorder of the RC. In the present study, we show evidence derived from a new analysis for rotational symmetry in 2D crystals that the reaction centre can be localised to four discrete orientations within the ring, and that only a single reaction centre is observable. In addition, we present evidence that the LHI ring is distorted from circular to square geometry.

Results

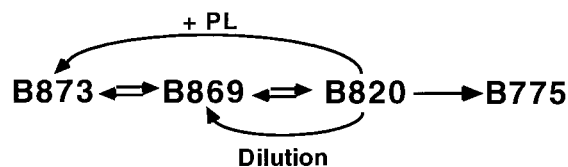
A titration of the spectral transitions of the RC-LHI complexes observed at room temperature with the increasing concentration of DHPC is shown in Scheme 1.

This profile is similar to that demonstrated previously (Kessi *et al.*, 1994, 1995) for preparations at room temperature, in that four discrete spectral forms (designated B873, B869, B820 and B775 according to their near-IR absorption maxima) are observed. The B820 and the B775 forms have been studied extensively by ourselves and others, and correspond to completely solubilised LHI-subunits of low molecular mass.

The near-IR/VIS absorption spectra of chromatophores in the presence of increasing amounts of DHPC are shown in Figure 1. The native chromatophores have a prominent absorption peak at 873 nm (B873). Careful stepwise addition of the detergent DHPC to a final concentration of 20 mM shifted this peak to 869 nm (B869). This shift was found to be reversible, when the detergent concentration was lowered below 2 mM DHPC, as was the case for dialysis against detergent-free buffer, as well as for direct dilution of solubilised complexes. At DHPC concentrations higher than 25 mM during solubilisation or 2.5 mM during the following purification steps, the spectral contribution due to B869 decreases in favour of an intermediate B820, which finally becomes B775. The latter transition was found to be irreversible. Crystallisation of the RC-LHI complexes was never possible from the B820 or B775 form.

Purification of RC-LHI

Initially, we employed the procedure of Kessi *et al.* (1994, 1995), also used by Walz & Ghosh (1997), for the preparation of 2D crystals. In this procedure, the DHPC-solubilised protein obtained from the chromatophore membranes is applied



Scheme 1.

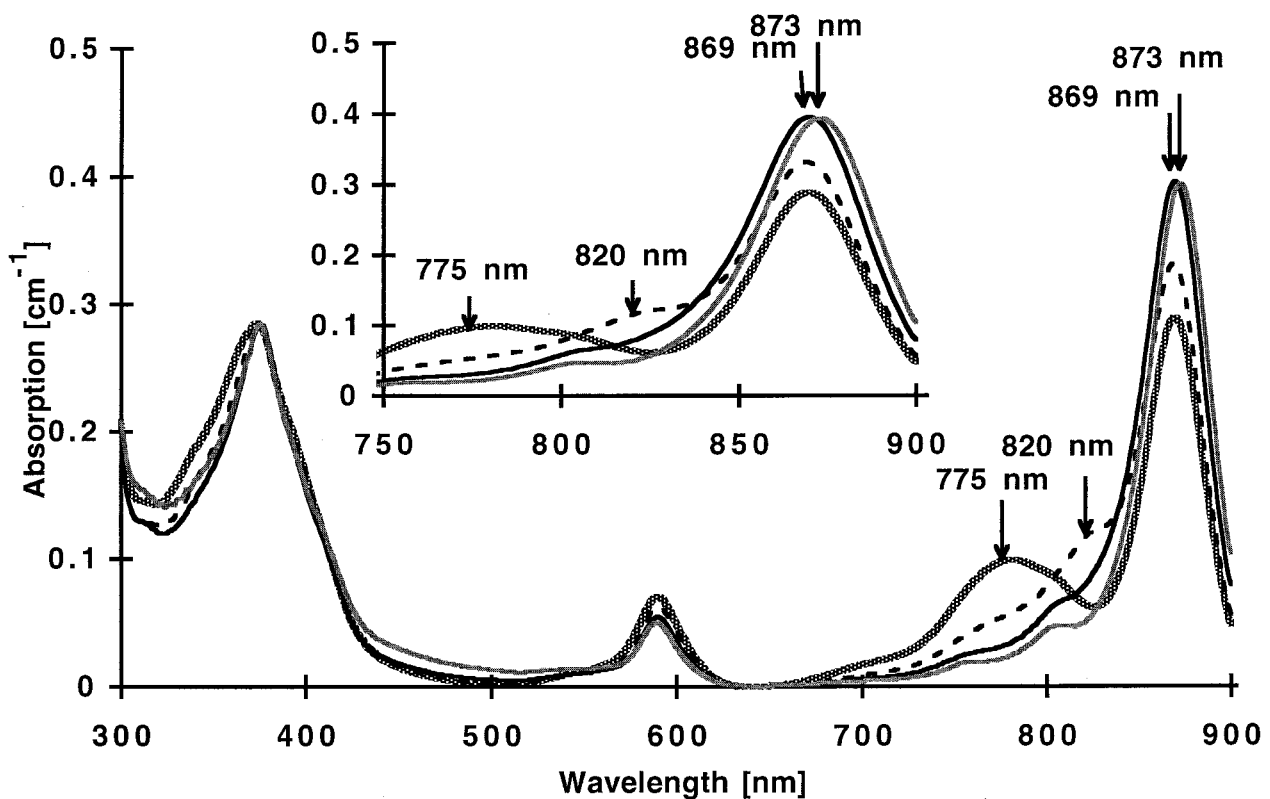


Figure 1. Absorption spectra of RC-LHI complexes (approx. 200 μg of protein) in the presence of varying amounts of DHPC are shown. The DHPC concentrations employed and the corresponding absorption maxima are indicated: 0 mM (—, 873 nm), 20 mM (—, 869 nm), 37 mM (---, 820 nm) and 374 mM (....., 775 nm). The inset shows an expansion of the region from 750 nm to 900 nm.

directly to a DEAE-Sepharose column, and the eluted fractions are used either directly, or are further purified using sucrose gradient centrifugation. In our hands, this procedure proved to be unreliable for routine crystallisation trials. The purity of the RC-LHI complexes obtained after the DEAE-Sepharose step is very variable with significant contamination by proteins with molecular masses above 30 kDa often observable. The employment of a sucrose gradient as the final step is effective in achieving a proper purification, but unfortunately leaves the final preparation in large quantities of sucrose that cannot easily and quickly be removed without disturbing the sensitive DHPC-RC-LHI equilibrium. In addition, the protein is always quite dilute at the end of this procedure, and thus requires a further concentration step prior to crystallisation.

By comparison, performing the sucrose gradient first is highly effective in removing the bulk of contaminating protein and the final DEAE-Sepharose step rapidly and reproducibly yields very pure and highly concentrated RC-LHI complexes in a buffer suited to crystallisation trials. The only difficulty we encountered with our final procedure was that during loading of the RC-LHI complexes obtained from the sucrose gradient onto the DEAE-Sepharose column, we often observed a dissociation of the complexes. We attributed this to a raising of

the local detergent concentration during binding to the column, possibly enhanced by the presence of large quantities of sucrose. Diluting the sucrose fractions with an equal volume of detergent-free and sucrose-free buffer immediately prior to DEAE-Sepharose loading proved to be an effective solution.

The most sensitive parameter for obtaining an optimal preparation suitable for crystallisation was the detergent concentration used during the purification. If the concentration of DHPC was too low, the RC-LHI complexes showed aggregation in transmission electron microscopy (TEM) images (not shown), and exhibited a corresponding shift of the B869 to the B873 form. If the concentration of detergent was too high, we observed spectral contributions due to B820 and B775 and found small particles without a defined shape using TEM (images not shown). In general, the diameter of the particles was below 10 nm. Subsequently the DHPC concentration was kept at 20 mM during solubilisation and at 2 mM during purification.

An SDS-PAGE gel (12.5% (w/v) acrylamide) of the variant steps of the RC-LHI purification is shown in Figure 2. The RD-LHI fraction shown in Figure 2, lane 6 was used for crystallisation. It shows the reaction centre subunits L, M and H at 12, 23 and 31 kDa. We assign the bands accumulated in the front to be the LHI subunits α and β .

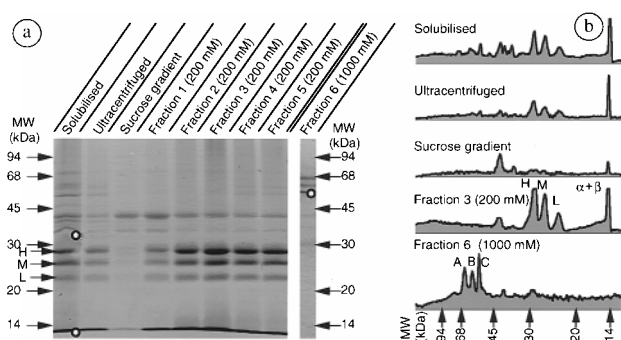


Figure 2. SDS-PAGE analysis of purified RC-LHI fractions. a, The lanes show (from left to right): 1, DHPC-solubilised membranes; 2, supernatant after ultracentrifugation following solubilisation; 3, the blue-green band observed after the sucrose gradient centrifugation; 4 to 8, collected fractions of the DEAE-Sephacrose column during elution with 200 mM NaCl. The fraction in lane 6 was used for crystallisation. 9, Fraction obtained during elution with 1000 mM NaCl. b, The protein profiles obtained by grey-scale densitometry of the SDS-PAGE gel are shown. The three heavy bands A (67 kDa), B (61 kDa) and C (57 kDa) observed for the fraction eluted with 100 mM NaCl as well as the RC subunits (H, M and L) are indicated. The open circles indicate the position of bands that stained positively for haem.

In all preparations we noted an unknown protein component with a molecular mass of 44 kDa. This protein begins to elute slightly ahead of the RC-LHI complex but is present also within the final preparation. However, our images of the crystal provide no evidence for a 44 kDa mass in addition to that of the LM subunit. We therefore assume that this component is either not present in the crystals or that it corresponds to incompletely dissociated LM dimers.

The last lane on the gel in Figure 2 was a fraction that was eluted with 1 M NaCl from the DEAE-Sephacrose column, after the column had been excessively washed with 200 mM NaCl. It shows three predominant bands at approximately 57 kDa, 61 kDa and 67 kDa. The 57 kDa band contained haem, as indicated by haem staining. We are unable to assign these bands at present. The final RC-LHI preparation obtained after the last DEAE-Sephacrose step could not be stained with the haem reagent. Other positive haem colorations are marked by circles.

A TEM image of negatively stained solubilised particles in the presence of detergent is shown in Figure 3a. The particles appear "banana"-shaped, have a width of $6.8(\pm 0.8)$ nm but are of variable length ranging from 12.8 nm to 40 nm or more.

Cryoelectron microscopy of single particles

Cryoelectron microscopy with a holey carbon film of the purified detergent-containing solution showed isolated particles that were frequently aggregated into one-dimensional arrays (Figure 3c).

Single particle analysis of the RC-LHI complexes

From preparations of isolated RC-LHI we removed the detergent by microdialysis as described in Materials and Methods. Negatively stained EM preparations were scanned for the occurrence of single particles that were neither aggregated nor included in crystal growth. An example of an image of single RC-LHI particles obtained in the absence of detergent is shown in Figure 3b.

In all, 788 images of single particles were collected from 67 negatives as described in Materials and Methods. A classification run rejected 118 images and grouped the remaining 670 images into four classes of 310, 202, 92 and 66 members. An average image for each class was calculated as shown in Figure 4. All four classes showed mainly the same appearance. In all classes, a stain-excluding bright ring was observed, which we attributed to the LHI ring. The differences between the four classes concerned mainly the extent of stain around the RC and were probably not significant. All classes showed the RC to be an elongated structure that separates the LHI ring into two halves. Figure 4i shows the rotational power spectrum obtained for the outer electron density along the LHI ring, as indicated in Figure 4a. The prominent peak at 4 shows clearly a distortion of the ring towards 4-fold symmetry.

Two-dimensional crystals of RC-LHI

Crystallisation was performed as described in Materials and Methods. After completion of the dialysis we found that the pH of the dialysis buffer had changed from 7.9 to 9.8. Electron microscopic images of negatively stained preparations of 2D crystal preparations with a range of lipid-to-protein ratios (*LPR*) between 0.75 and 1.33 (mol DOPC to mol LHI) are shown in Figure 5. Crystalline membrane patches were observed that were covered to a varying extent with small pure lipid vesicles of about 100 nm diameter. Samples with *LPR* of both much lower and much higher than 1.0 showed only a low density of pure lipid vesicles, while sample with *LPR* close to 1.0 showed the greatest amount of the vesicles. The quality of the crystals found in a sample tube was always in direct correlation with the density of these vesicles. The best crystals were found in preparations with the highest amount of phospholipid vesicles and at a lipid to protein molar ratio of 1.0. Images for structure reconstruction were recorded for samples where the vesicles had been removed by centrifugation.

Conventional image treatment of 2D crystal images

Image treatment was done as described in Materials and Methods. The result is shown in

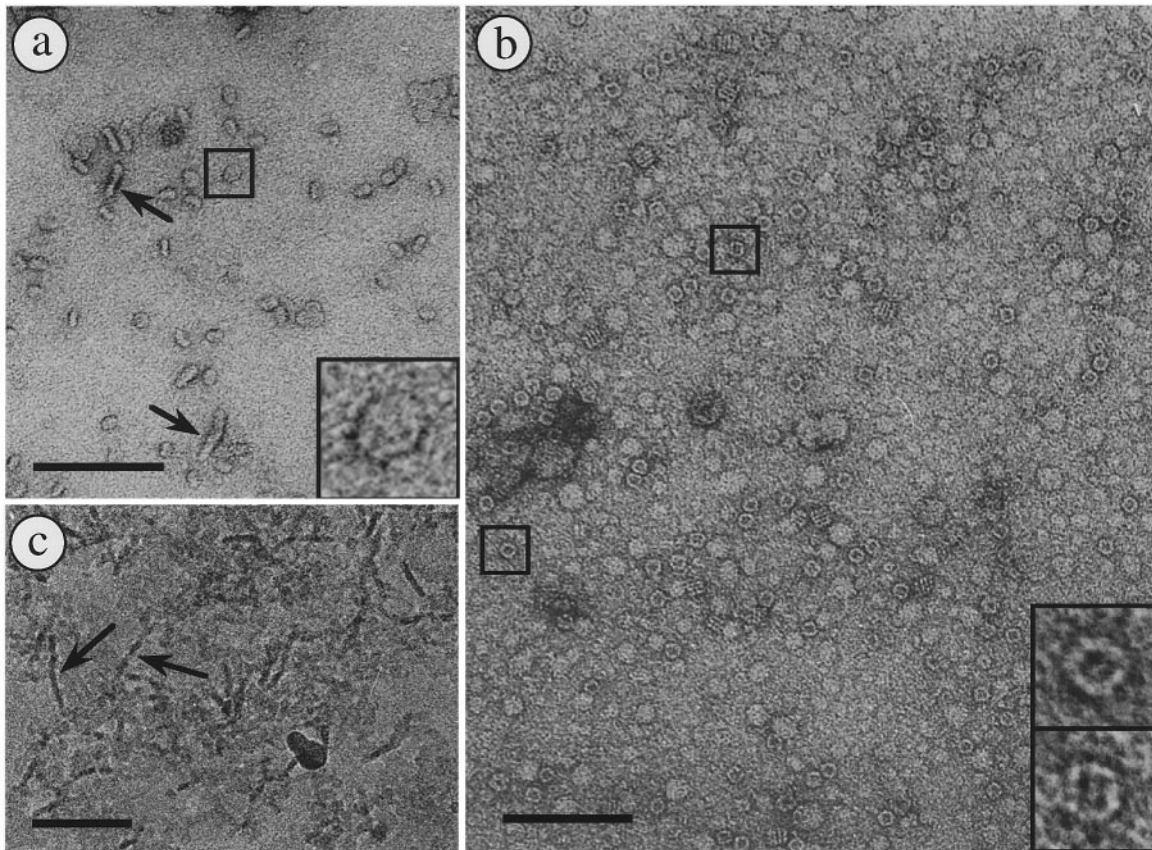


Figure 3. TEM images of purified RC-LHI complexes. a, A negatively stained preparation shows the complexes that frequently formed one-dimensional “banana”-shaped aggregates (arrows). Isolated particles appear round in the presence of detergent (a) and squarish in its absence (b). The latter is rare to find, since most of the particles will be aggregated. c, A cryoelectron microscope image of the same preparation as in a with detergent in the absence of stain, using the holey carbon film technique. Here, no conclusion can be made about the square or round shape of the complexes, but one-dimensional aggregations of complexes are visible (arrows). Scale bars represent 100 nm. The insets show selected particles at 4× magnification.

Figure 6. The images show that the RC-LHI complexes are arranged in a square lattice with the lattice dimensions of $16.65(\pm 0.1)$ nm, which is in agreement with the observations by Walz & Ghosh (1997), who obtained 16.3 nm as the lattice dimensions. As observed by Walz & Ghosh (1997), the adjacent RC-LHI complexes are arranged in a head-to-tail packing with one face of the complex apparently protruding into the aqueous layer. In the preparation reported here, only small amounts of negative stain were employed, thus visualising the region between the carbon film support and the membrane surface. Objects protruding from the membrane surface towards the support therefore appear lighter. As the RC of *R. rubrum* contains only the cytoplasmically located H-subunit and no tightly bound cytochrome subunit, we have assigned the lighter, protruding face to the cytoplasmic side (C) and the darker, flatter side to the periplasmic side (P) of the RC-LHI complex in Figure 6d. In the crystals analysed we found no sign of “empty” LHI rings.

RC-LHI complexes appear to have a square-like structure for the LHI ring on both sides of the membrane. On the cytoplasmic side, the reaction centre appears in the reconstruction mainly rounded with a bias towards a 4-fold symmetry. On the periplasmic side, the RCs show a low profile, which is at about the same height as the surrounding membrane. Again there is a weak 4-fold symmetry observable in its reconstruction (Figure 6e). The rotational power of spectra obtained for the electron density of the periplasmic and cytoplasmic sides of the LHI rings are indicated in Figure 6d and given in Figure 6g. The prominent peak at the fourth rotational power again indicates a 4-fold symmetry for the LHI ring. The power spectrum for the periplasmic side and, to some extent, that for the cytoplasmic side show a stronger peak at 16, which we attribute to the $16\alpha\beta$ subunits in the LHI ring. Preliminary analysis of the RC-LHI crystal structure by cryoelectron microscopy with a continuous carbon film revealed a similar square-like structure, though at lower resolution (Figure 6h).

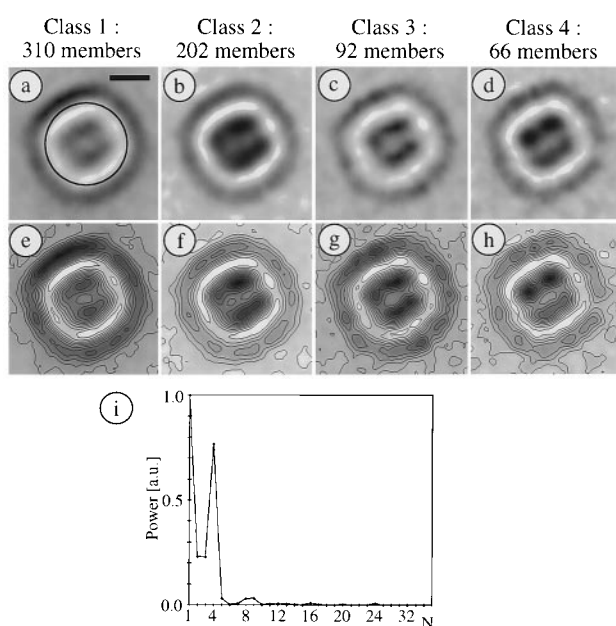


Figure 4. A projection average of single purified RC-LHI particles obtained by multivariate statistical analysis. Of 788 single particles, 670 were classified into four classes. The average of the images of each group is shown in grey-scale (a to d) and in contour representation (e to h). The negative stain appears as dark, the bright stain-excluding regions correspond to protein. No symmetry was assumed during image treatment. The scale bar in a represents 5 nm. The rotational power spectrum for the electron density of the LHI ring, indicated by a circular line in a, is shown in i.

Rotational single particle analysis of 2D crystals

The reaction centres within the crystal were aligned as described in Materials and Methods. The angular distributions of the completely free and the 16-fold free rotational searches repeatedly showed four clear maxima, separated by 90° (Figure 7f). This result led us to assume that each RC within the RC-LHI crystal has one of four possible orientations, thus enabling the possible rotation angles to be fixed to a multiple of 90° . The resulting image for the periplasmic side of the reaction centre is shown in the centre of Figure 7e. The reconstructions for the neighbouring RCs in Figure 7e remain as before, indicating no orientation correlation among neighbouring RCs. This procedure was applied separately to a set of images centred around the bright RCs inserted in the crystal, as well as to a set of images centred around the darker RCs in the crystal, which we assign to the cytoplasmic and periplasmic sides of the RCs, respectively. A collage of both reconstructions of the cytoplasmic side is indicated in Figure 8a by arrows. No local correlation between neighbouring units was ever observed.

Attempts to rotationally align the masked LHI rings alone resulted in no deviation of the closed ring structure (data not shown).

Discussion

For highly purified LHI from *R. rubrum*, the B873 form has been shown to correlate exclusively

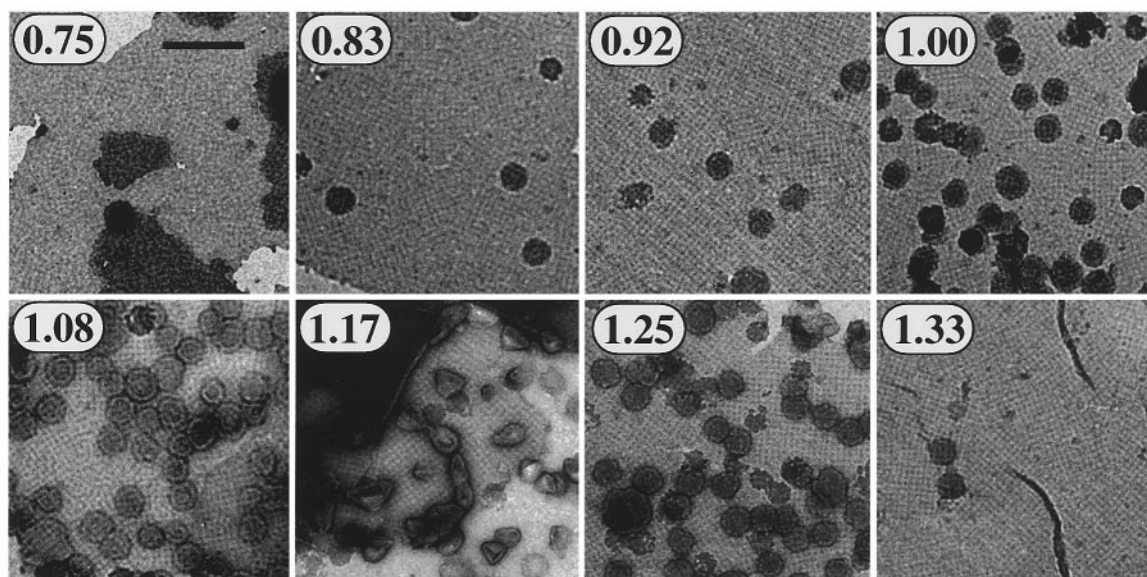


Figure 5. TEM images of negatively stained crystallisation preparations with different lipid to protein ratios are shown. In order to crystallise the purified photounits, a series of lipid to protein ratios (*LPR*) were dialysed. The corresponding *LPR* values (mol DOPC/mol LHI) are indicated. The largest and most coherent crystals were obtained at a molar ratio of about 1.0. The quality of the crystals was always correlated with the density of pure lipid vesicles. At higher (*LPR* 0.75) and at lower (*LPR* 1.33) lipid to protein ratios than optimal, a lowering of the crystal quality appeared to parallel the disappearance of small pure lipid vesicles. The scale bar represents 200 nm.

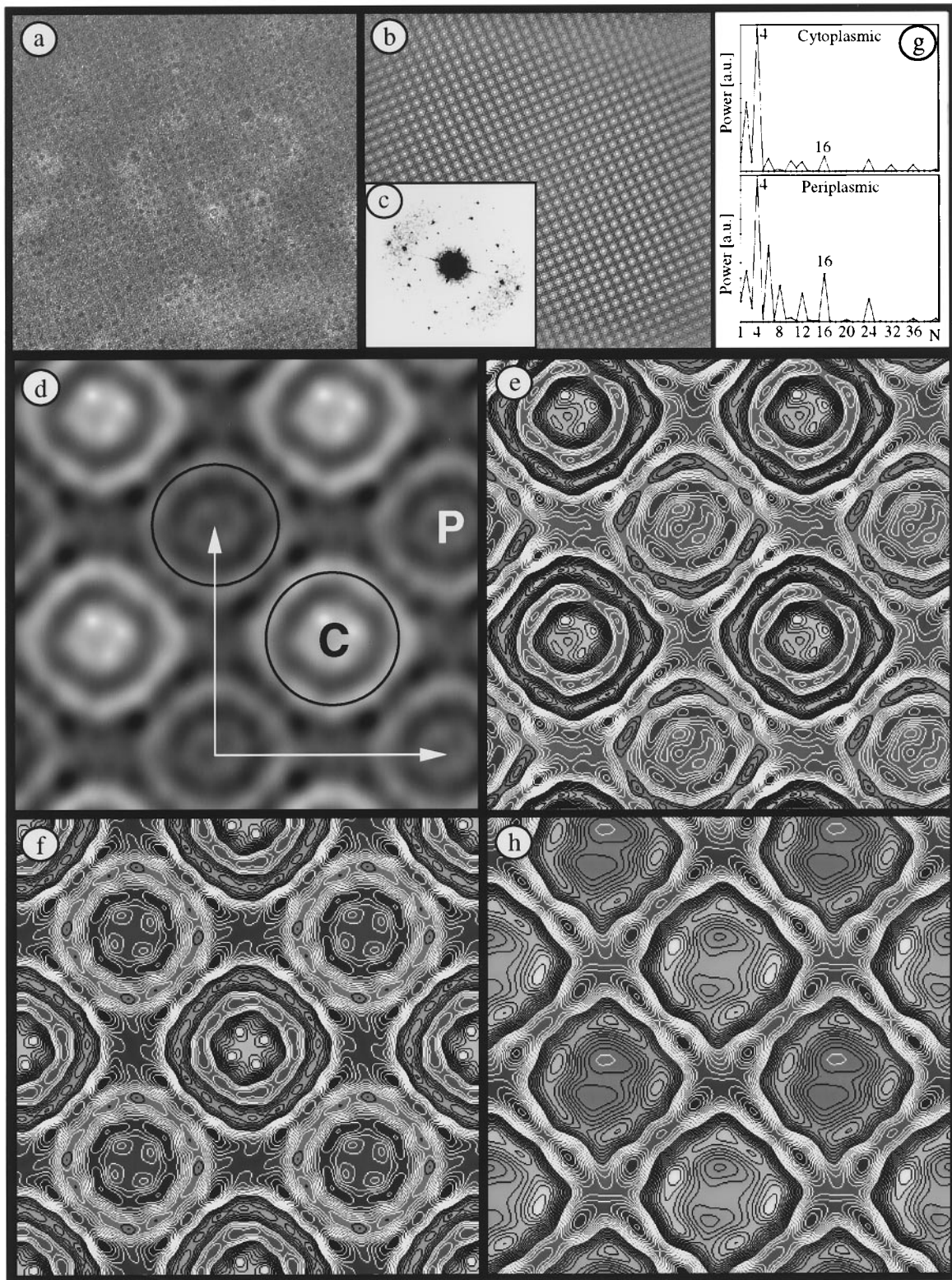


Figure 6. The “conventional” analysis of the TEM images of 2D crystals of RC-LHI complexes. a, A TEM image of a negatively stained 2D-crystal. b, The same image after Fourier-filtering. c, The calculated diffraction pattern of a. d and e, Projection maps calculated to 1.6 nm resolution from a, using the MRC software for image treatment show the unit cell to contain two photounits, one facing the cytoplasmic side (marked with C) and one with the periplasmic side towards the grid (marked with P). The cell dimensions are $a = b = 16.65(\pm 0.1)$ nm, which corresponds to a mean diameter per photounit of $11.77(\pm 0.07)$ nm. No symmetry operation was applied here. f, Projection map obtained after 4-fold ($p4$) symmetrisation of the structure shown in d. g, The rotational power spectra calculated for the electron densities along the periplasmic and cytoplasmic sides of the LHI rings as indicated in d. h, Image reconstruction from an RC-LHI crystal image recorded using cryoelectron microscopy with a continuous carbon film support. Since the crystal is mainly embedded in the vitrified suspension, the differences between the two orientations of the units are less visible. This reconstruction has a worse resolution than d.

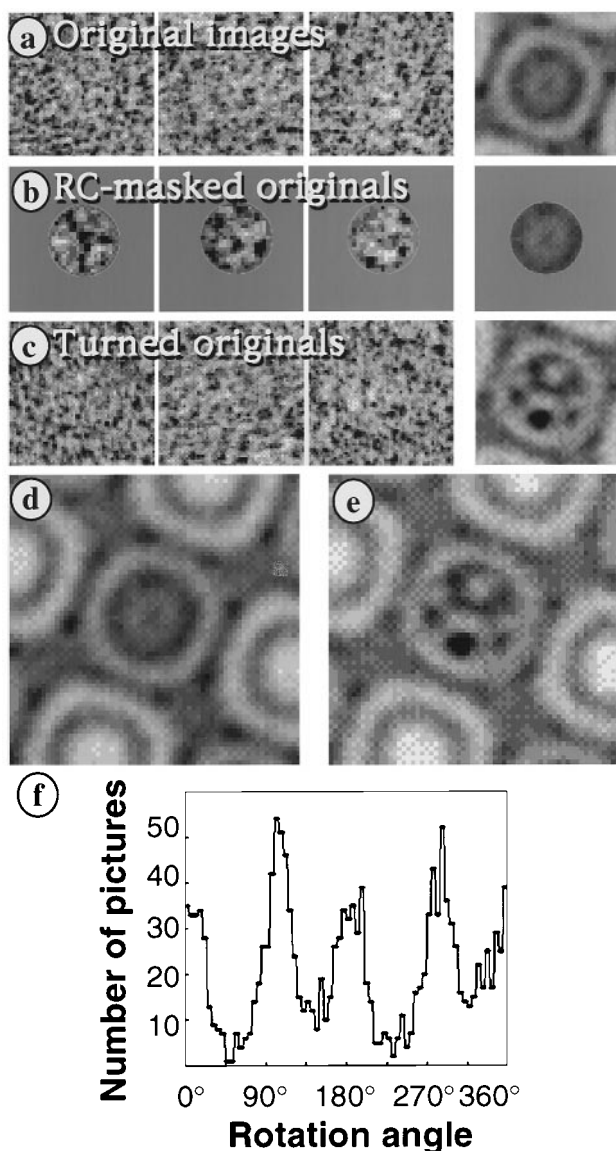


Figure 7. The scheme of the modified image treatment algorithm for rotational alignment of the RCs. a, A series containing 2700 images was obtained by cross-correlation methods; the first three images are shown to illustrate the method. The fourth horizontal image is the average of the series. The direct average of these images gives the so-called classical reconstruction (topright corner). b, The images were masked with a radius corresponding to the inner diameter of the LHI ring. The masked images were used to determine the rotation of each RC by cross-correlation. Again, the average of this series is shown as the last horizontal box. c, Using the angles obtained from the masked images, the original images were rotated accordingly (first three boxes in c) and averaged (last box in c). The average of these turned images gave the so-called rotational reconstruction. d and e, The classical reconstruction and the rotational reconstruction using a set of larger images. f, The angular distribution of the masked images. Four maxima are visible, separated by 90°, indicating that the RC can occupy four fundamental orientations within the RC-LHI crystal.

with a vesicular aggregate of the complex (Ghosh *et al.*, 1988a,b; 1990). This has been confirmed here from images of negatively stained preparations and by sucrose gradient centrifugation of the RC-LHI complexes described here. The B869 form has been observed for isolated LHI complexes after rapid dilution of β OG-solubilised B820 complexes. Images obtained from negatively stained LHI-B869 showed banana-shaped particles identical with

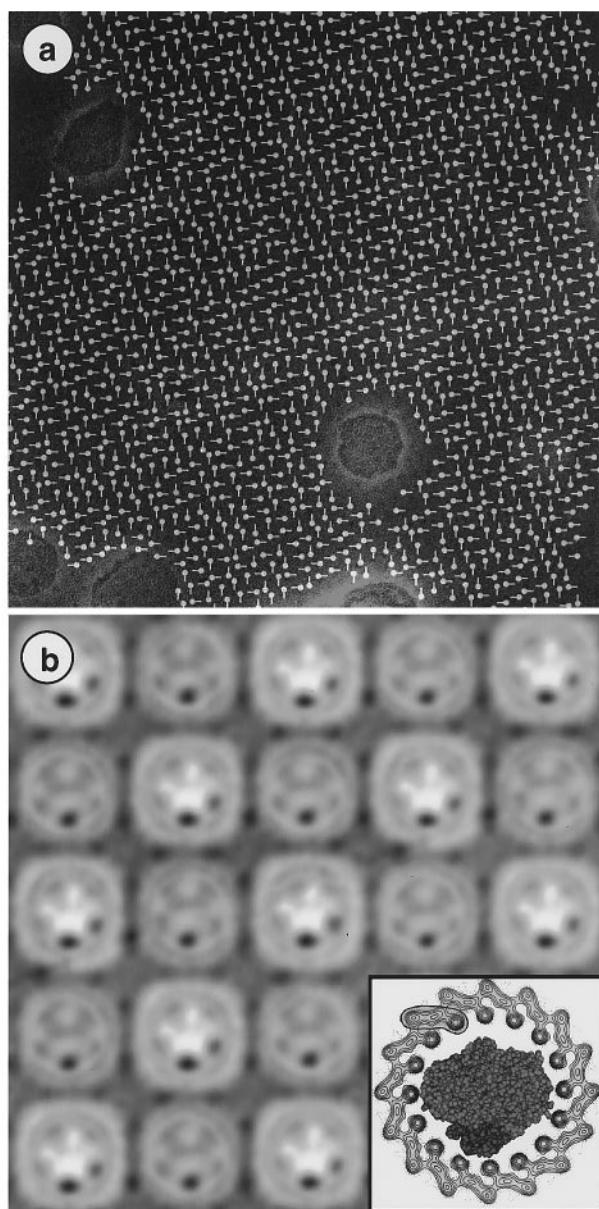


Figure 8. The results of the rotational RC-alignment. The local angular distribution of the RCs is indicated in a. One of four possible orientations, separated by 90°, was allowed in this correlation search. No correlation between the rotation angles of neighbouring reaction centres was ever observed. Cytoplasmic and periplasmic sides of the RC were treated independently. A collage of the image treatment results is shown in b. The inset is an RC-LHI model based upon the RC structure of *R. sphaeroides* (Allen *et al.*, 1987) and the projection map of LHI of *R. rubrum* (Karrasch *et al.*, 1995).

those shown here for the RC-LHI complexes and as demonstrated by Kessi *et al.* (1995). However, we have observed repeatedly that any red shift of the absorption peak maximum at 869 nm (B869) towards 873 nm during the purification is always associated with a partial or complete large-scale aggregation of photounits and is always fatal to crystallisation. We have therefore selected conditions for purification and crystallisation where the B869 form of the RC-LHI complex was predominant if not exclusive.

In this study, we initially examined solubilised and purified single RC-LHI units by electron microscopy. The images from negatively stained preparations confirmed the observations by Ghosh *et al.* (1990) and Kessi *et al.* (1995) that the B873 and B869 forms of the solubilised RC-LHI complexes corresponded to vesicular aggregates and banana particles respectively. The solubilised particles showed a width of $6.8(\pm 0.8)$ nm and a length ranging from 12.8 nm to 40 nm. In our study, however, we were able to confirm that the B869 to B873 transition corresponds exclusively to the aggregation of the B869 complex. Thus, sucrose gradients employing less than 2 mM DHPC resulting in a red shift of the maxima at 869 nm were always associated with an increase in the observed density of the complex corresponding to that of non-dissociated RC-LHI (B873). Bands isolated from these gradients contained arrays of particles as judged by TEM imaging after negative-staining. The DHPC-solubilised banana RC-LHI particles have the same appearance when examined by cryoelectron microscopy with samples immobilised in ice using the holey carbon film technique (Figure 3c). The images in cryoelectron microscopy appear to be one-dimensional aggregates of particles of 12 to 15 nm widths.

TEM images of negatively stained photounits without detergent displayed square-like particles with an outer diameter of $11.0(\pm 0.7)$ nm. This apparent conflict with the observations by Boonstra *et al.* (1994), who observed the RC-LHI complexes of *R. molischianum* to be of cylindrical shape, might be due to the lower resolution of the data in *R. molischianum*, which were recorded in the presence of detergent.

Our reconstruction indicates 16 $\alpha\beta$ subunits in the LHI ring in good agreement with the LHI projection structure obtained by Karrasch *et al.* (1995); see Figure 6g. We note that the latter study was performed with wild-type LHI complexes, whereas our study has employed a carotenoid-less mutant. These data indicate that the presence of carotenoid does not influence the aggregation state of the complex.

Perusal of the large number of images obtained from negatively stained RC-LHI particles suggests that the particles have a strong tendency to adsorb with the cytoplasmic side facing towards the supporting hydrophilic carbon film. The similar orientation towards the support could explain the fact that the major part of the scanned par-

ticles were classified into similar classes. The particles therefore show a projection in the reconstruction that is comparable to the observed 2D crystal projection for the cytoplasmic side of the complexes.

Single particle alignment of the RC in the crystal lattice of the LHI rings was done here for the first time. The RCs alone would be much too small to allow a single particle treatment from negatively stained preparations. Here, we had the peculiar situation that the position of each RC was fixed and known quite accurately, thus leaving the rotational angle as the only degree of freedom to be determined. The alignment was greatly facilitated by the empirical finding that the RC was restricted to four possible orientations in the crystal.

We believe the RCs to have one of four possible orientations in the crystal because of the following reasons. (1) The "classical" reconstruction of the 2D crystal structure using SEMPER or the MRC program suite shows for the RC a square-like structure, which indicates a superposition of four discrete orientations. (2) Rotational alignment of the RCs without the LHI rings, using either a completely free or a 16-fold free rotation angle shows an angle distribution containing four peaks, each separated by 90° . (3) The analysis of stained and unstained single RC-LHI particles yielded a square symmetry with a non-symmetrical projection for the RC. This can be explained only if one assumes a fixed orientation of the RC towards one of the four sides of the LHI ring. As the square-like LHI rings are inserted in the 2D crystal in one of four orientations, this must hold true for the RCs.

This analysis raises the question: is the square-like shape of the LHI ring from the carotenoid-less mutant an intrinsic property of the ring or is it induced by the presence of a reaction centre?

The unit cell packing observed in this study of 2D crystals of the RC-LHI complex is essentially identical with that presented by Walz & Ghosh (1997), although the resolution obtained in the latter study was somewhat less than that shown here, only the conventional analysis (i.e. non-rotated direct cross-correlational averaging) was performed. Nevertheless, these authors were able to demonstrate that 2D crystals formed from the LHI complex in the absence of reaction centre show a unit cell packing identical with those containing reaction centre. This strongly suggests that the square packing is determined exclusively by the interaction between carotenoid-less LHI rings. The square geometry of the rings in these complexes provides a simple explanation for the observation that the reaction centre is located in the LHI ring in one of four elementary rotations. Even at the presently attainable resolution of the 2D crystals shown here, the LHI ring shows an elementary symmetry of 16 (Figure 6g). This

indicates that the structure of the carotenoid-less LHI ring is not fundamentally different from that of the wild-type LHI complex and is also composed of 16 $\alpha\beta$ pairs. If the geometry is square however, then the "diameter" corresponds to the length of a "side", which must be smaller than the diameter of a circle composed of the same number of subunits and the "diagonal" of the square must be correspondingly larger. The distortion of the carotenoid-less LHI ring (which even for the wild-type circular form is only just sufficient to incorporate a single reaction centre) to a square geometry, might therefore force the reaction centre to assume one of four orientations solely on the basis of steric interactions. An equally likely possibility is that the fixed interaction of the reaction centre with the LHI ring at a single locus facilitates the distortion of the LHI ring at that point when packed in a crystal.

A central question is: what factor causes a circular structure with perfect 16-fold to form a square geometry? Clearly, a mechanism that could explain this phenomenon is that the energy of interaction between $\alpha\beta$ subunits is lowered at four loci due to the presence of an additional factor, possibly a further protein species. A possible candidate for the additional molecule(s) in the LHI ring may be the 4 kDa polypeptide Ω (Ghosh *et al.*, 1994), as suggested previously (Walz & Ghosh, 1997). Why four (or a multiple thereof) additional protein subunits, possibly Ω , should bind at loci equidistant from each other, cannot be answered at this time.

An alternative mechanism for the square geometry might be that the interactions between carotenoid-less LHI rings during the early stages of crystallisation occurs with $p4$ symmetry and that lateral pressure within the bilayer membrane during the final stages of crystallisation cause the rings to distort to a square geometry. This hypothesis is based upon the observation that for 2D crystals from the wild-type LHI complex, a 4 to 6% distortion from the unit cell was observed (Karrasch *et al.*, 1995) and it has been shown that the carotenoid-less complexes are less stable than those of the wild-type, suggesting a weaker interaction between $\alpha\beta$ pairs.

However, the observation that even single particles of the RC-LHI complex show a square geometry suggests that the latter hypothesis may not be correct and that the square packing observed in the crystal is a natural consequence of packing of the individual square-like LHI ring units. At this point, we still cannot answer the question as to why the LHI and RC-LHI rings of the carotenoid-less mutant appear to have a geometry different from that of the wild-type. We expect that studies of 2D crystals diffracting to higher resolution will shed light on this question.

Materials and Methods

Chemicals

All chemicals were of the highest purity available and, in general, were obtained from Fluka Chemie AG (Buchs, Switzerland). Exceptions were: 1,2-diheptanoyl-*sn*-phosphatidylcholine (DHPC from Avanti Polar Lipids, Alabaster, AL); DEAE-Sepharose CL-6B (from Pharmacia, Dübendorf, Switzerland); β -octylglucoside (β OG from BACHEM, Bubendorf, Switzerland). Solutions for silver staining were from BioRad.

Growth of *R. rubrum* and preparation of chromatophore membranes

The carotenoid-less Tn5 mutant *R. rubrum* ST2 (Wiggli *et al.*, 1996) was grown in 20 litre bottles in dim light and under anaerobic heterotrophic conditions using Sistrom medium A (Sistrom, 1977) as described (Saegesser *et al.*, 1992) and harvested as described (Wiggli *et al.*, 1996). They were quick-frozen in liquid nitrogen and stored at -80°C .

Purification of the RC-LHI complex

The solubilisation and purification of the RC-LHI complex was performed using a modification of the procedure of Kessi *et al.* (1995). Chromatophores were suspended in buffer A (10 mM Tris-HCl (8.0), 150 mM NaCl, and 2 mM MgCl_2 to $A_{873}(1\text{ cm}) = 20$ as measured from a 20-fold diluted sample. Diheptanoyl-*sn*-phosphatidylcholine (DHPC) was added constantly over ten minutes to a final concentration of 20 mM at room temperature. The solution was allowed to equilibrate with stirring for 20 minutes at room temperature. An absorption spectrum showed that the absorption peak maximum at 873 nm (B873) had shifted to 869 nm (B869). The DHPC-solubilised RC-LHI particles were obtained as the supernatant following ultracentrifugation at 120,000 g for one minute at 4°C . The solubilised material was loaded onto a sucrose gradient (0.4 M to 2.0 M) in buffer A containing 2 mM DHPC and the gradient was then centrifuged for 36 hours at 100,000 g at 8°C . After centrifugation, a single band was visible at a density corresponding to approximately 1 M sucrose. The band was collected and applied to a DEAE-Sepharose column, which had been equilibrated with buffer A containing 2 mM DHPC. The column containing the bound RC-LHI complexes was washed with two column volumes of the equilibration buffer and the complexes were eluted with the same buffer containing 200 mM NaCl (elution buffer). Fractions were collected and stored at 4°C .

To prevent photo-oxidation, all purification and crystallisation steps were done in dim light and under a nitrogen-enriched atmosphere. All buffer solutions and the sucrose gradients were purged with nitrogen gas prior to use.

Two-dimensional crystallisation of the RC-LHI complexes

For 2D crystallisation, approximately 200 μg of the purified photounits plus the phospholipid dioleoyl-*sn*-phosphatidylcholine (DOPC) in a series of molar ratios of DOPC to LHI from 0.75:1.0 to 1.33:1.0 were adjusted to a volume of 100 μl with elution buffer. The con-

centration of the stock suspension of phospholipids was determined by the ammonium molybdate method. The suspension was sonicated to clarity immediately prior to mixing with the RC-LHI complexes obtained directly from the DEAE-Sepharose column. Dialysis was performed for six days at 8°C in microdialysis setups against 2.4 ml of buffer B (50 mM NH_4HCO_3 (pH 7.9), 200 mM NaCl, 10 mM MgCl_2) and containing 0.8% (w/v) βOG . A second dialysis of seven days followed against 2.4 ml of buffer B at 8°C. Crystallisation procedures were performed in a Plexiglas box, which allowed the entire handling to be done in dim light and under a nitrogen-enriched atmosphere. The 2D crystals were separated from small vesicles by centrifugation at 13,000 g for one minute and carefully resuspending the pellet in dialysis buffer. The crystals were fixed onto electron microscopy grids by the standard negative-staining procedure or by plunge-freezing into liquid ethane within eight hours after collection. Grids with crystals older than 24 hours after collection showed significantly worse diffraction in the microscope.

Preparation of single RC-LHI particles

For the microscopic imaging of detergent-free single photounits, various amounts (10 to 200 μg) of the purified material were directly dialysed against 2.4 ml of buffer B for 14 days. The solution was then centrifuged at 15,000 g for one minute in order to remove crystals and aggregates. The supernatant was prepared by negative-staining and screened for single particles.

Absorption spectroscopy

Absorption spectra from various samples were obtained between 250 nm to 900 nm with a JASCO 550 IR/VIS spectrometer equipped with a custom-built cuvette-holder for the minimisation of stray light. Signal detection was performed using photodiodes with extended sensitivity in the near-IR region placed close to the sample and reference cuvettes, respectively.

Preparation of samples for SDS-PAGE

The protein concentration of the samples was determined by a modified Lowry method for the analysis by SDS-PAGE of membrane protein (Peterson, 1977).

Samples were precipitated by the addition of three volumes of 75% (v/v) methanol, allowed to equilibrate at room temperature for 20 minutes, then centrifuged at 15,000 g for 20 minutes. After removal of the supernatant, the pellet was resuspended in 20 μl of 60 mM Tris-HCl (pH 6.8), 5% (v/v) glycerol, 2% (w/v) SDS, 0.003% (w/v) bromphenol blue, 10 mM EDTA, 200 mM dithiothreitol, then vortex-mixed for 30 seconds, heated to 95°C for 90 seconds and vortex-mixed again for 30 seconds. The supernatants were centrifuged for five minutes at 15,000 g, then analysed by SDS-PAGE according to Laemmli (1970). Visualisation was performed by Coomassie Blue R250 staining, silver staining (BioRad) and haem staining (Thomas *et al.*, 1976; Goodhew *et al.*, 1986).

Transmission electron microscopy

Drops of 3 μl of the solutions were applied onto carbon-coated 400-mesh copper grids that had been rendered hydrophilic by glow discharge. The drops were

allowed to adsorb onto the carbon film for between five seconds and five minutes, depending on the quantity of material in the solution. This was performed in dim light and in a humid atmosphere to avoid evaporation. For negatively stained, grids, the drop was blotted from the edge of the grid and then stained with 2% (w/v) uranyl acetate (pH 4.2) without prior washing. After ten seconds the grid was blotted from the edge, air-dried and stored under vacuum.

For cryoelectron microscopy, a 3 μl drop was applied to a copper grid that had been covered with a platinum-coated holey carbon film. The drop was blotted for three seconds with filter-paper touching the grid surface. Alternatively, a continuous carbon film-coated grid was used, which had been rendered hydrophilic by glow discharge. A drop was allowed to adsorb onto the carbon film for between five seconds and five minutes and blotted for one minute in a humid atmosphere. The grids were then plunged immediately into liquid ethane, kept at its freezing point by liquid nitrogen and stored in liquid nitrogen (Adrian *et al.*, 1984; Dubochet *et al.*, 1988).

Transmission electron microscopy (TEM) was carried out with a Philips CM12, operated at 80 kV with an objective aperture of 100 μm always in place. Negatively stained grids were examined using a standard room temperature holder. Grids for cryoelectron microscopy were transferred to a Gatan 626 cold stage and examined at -172°C. Images were recorded under low-dose conditions at nominal magnifications of 45,000 \times on Kodak SO-169 plates, which were developed in D19 standard developer for ten minutes. The electron dose for acquiring an image was between 500 and 1000 electron/nm².

Image treatment

Micrographs were examined with an optical diffractometer (Aebi *et al.*, 1973) and suitable areas were digitised using an Eikonix 850 CCD imaging camera. The pixel size corresponded to 0.36 nm in the specimen plane, the digitised images contained 4096 \times 4096 pixels.

Single particles

Images of single particles were treated using the programs SPIDER and WEB (Frank *et al.*, 1985; Radermacher, 1988). The reference-free algorithm of Penczek *et al.* (1992) was used for particle alignment. The images were classified using multivariate statistical analysis methods and averages of each class were calculated (Van Heel, 1984; Frank *et al.*, 1987; Harauz *et al.*, 1988).

2D crystals

"Classical method". Images were treated using the cross-correlation method with SEMPER6 (Saxton *et al.*, 1979; Saxton, 1996) as described by Walz *et al.* (1994). In parallel, a software package distributed by the MRC (Cambridge, UK) was employed (Henderson *et al.*, 1986, 1990).

Rotational single particle analysis of 2D crystals. To correct for the differing orientations of the RCs in each LHI ring, a new image treatment was developed, which is essentially a combination of the methods described above. To obtain the exact locations of the RC-LHI unit cells in the crystal, the raw image of 4096 \times 4096 pixels was unbent with the unbending

routine from the MRC software package. This unbent image was then treated with SEMPER6. Fourier-filtering produced an approximate reference image for the RC-LHI structure, which was used for a cross-correlation search in the image. The peaks in the cross-correlation map indicated the exact locations of the RC-LHI unit cells with the still non-oriented RCs. The obtained list of co-ordinates together with the unbent image were then used in the program SPIDER. A windowing operation cut, at each indicated unit-cell location, a small image of 128×128 pixels. This produced a set of a few thousand small images that were each exactly centred over one RC-LHI unit cell.

This set of images was rotationally aligned using an individual rotation angle for each image. This corresponds to a single particle treatment with exactly known lateral positions and the rotation angle as the only degree of freedom. This missing rotation angle was determined by cross-correlation against a reference. In order to be influenced only by the RC's orientation, the LHI rings and the rest of the images were covered by a circular mask that had a diameter corresponding to the inner border of the LHI ring (Figure 7b). The masked images were then rotational cross-correlated against a reference. The optimal rotation angle was determined for each small masked image. This set of angles was then used to rotate the original, unmasked set of small images (Figure 7c). The rotated images of this set were then averaged, resulting in the rotationally corrected reconstruction (Figure 7e).

For the rotational cross-correlation of the masked small images, several different references were tested. The result of the single particle treatment or one representative member of the set of small images or arbitrarily created synthetic patterns was used. Also, a reference-free alignment procedure as described (Penczek *et al.*, 1992) was employed. The aligned images resulted in a reconstruction, which was recursively used as the new reference until the obtained reconstructions had converged to a final structure. During the rotational alignment, different border conditions were allowed: the rotational angles were allowed to have any free value or a multiple of $360^\circ/16$ or a multiple of $360^\circ/4$.

In further trials, the outside and the inside of the LHI rings were masked in order to look for inhomogeneities in the LHI ring alone. Such an inhomogeneity might, for instance, be a gap in individual non-oriented LHI rings, which would not be detectable by conventional image treatment on 2D crystals due to averaging.

Rotational power spectra

The grey-scale distribution obtained for the electron density along the LHI ring (a circular line) was transformed into polar coordinates, Fourier-transformed, and the power spectrum was calculated using the program SEMPER6.

Acknowledgements

We thank Per Bullough and Thomas Walz for their help with the image analysis with the MRC software and for stimulating discussions. We thank Marie-France

Blanc for expert technical assistance and Reto J. Strasser for encouragement and support. We acknowledge the Swiss National Science Foundation Priority Program on Biotechnology, grants no. 5002-35180 to H.S. and H.V. and nos 5002-41801 and 5002-39816 to R.G. for generous financial support.

References

- Adrian, M., Dubochet, J., Lepault, J. & McDowell, A. W. (1984). Cryo-electron microscopy of viruses. *Nature*, **32**, 32–36.
- Aebi, U., Smith, P. R., Dubochet, J., Henry, C. & Kellenberger, E. (1973). A study of the structure of the T-layer of *Bacillus brevis*. *J. Supramol. Struct.* **1**, 498–522.
- Allen, J. P., Feher, G., Yeates, T. O., Komiya, H. & Rees, D. C. (1987). Structure of the reaction centre from *Rhodobacter sphaeroides* R-26: the cofactors. *Proc. Natl Acad. Sci. USA*, **84**, 5730–5734.
- Boonstra, A. F., Germeroth, L. & Boekema, A. (1994). Structure of the light-harvesting antenna from *Rhodospirillum molischanum* studied by electron microscopy. *Biochim. Biophys. Acta*, **1184**, 227–234.
- Deisenhofer, J. & Michel, H. (1989). Nobel lecture. The photosynthetic reaction centre from the purple bacterium *Rhodospseudomonas viridis*. *EMBO J.* **8**, 2149–2170.
- Deisenhofer, J., Epp, O., Miki, K. H. & Michel, H. (1985). Structure of the protein subunits in the photosynthetic reaction centre of *Rhodospseudomonas viridis* at 3 Å resolution. *Nature*, **318**, 618–624.
- Drews, G. (1985). Structure and functional organization of light-harvesting complexes and photochemical reaction centres in membranes of phototrophic bacteria. *Microbiol. Rev.* **49**, 59–70.
- Dubochet, J., Adrian, M., Chang, J. J., Homo, J. C., Lepault, J., McDowell, A. W. & Schultz, P. (1988). Cryo-electron microscopy of vitrified specimens. *Quart. Rev. Biophys.* **21**, 129–228.
- Engelhardt, H., Engel, A. & Baumeister, W. (1986). Stoichiometric model of the photosynthetic unit *Ectothiorhodospira halocloris*. *Proc. Natl Acad. Sci. USA*, **83**, 8972–8976.
- Fernández-Velasco, J. & Crofts, A. R. (1991). Complexes or super-complexes: inhibitor titrations show that electron transfer in chromatophores from *Rhodobacter sphaeroides* involves a dimeric UQH₂:cytochrome *c*₂ oxidoreductase, and is delocalized. *Biochem. Soc. Trans.* **19**, 588–593.
- Frank, J., Verschoor, A. & Wagenknecht, T. (1985). Processing of electron-microscopic images of single macromolecules. In *New Methodologies in Studies of Protein Conformation* (Wu, T. T., ed.), pp. 36–89, Van Nostrand-Reinold Inc., New York.
- Frank, J., Breaudiere, J.-P., Carazo, J.-M., Verschoor, A. & Wagenknecht, T. (1987). Classification of images of biomolecular assemblies: a study of ribosomes and ribosomal subunits of *Escherichia coli*. *J. Microsc.* **150**, 99–115.
- Ghosh, R., Hauser, J. & Bachofen, R. (1988a). Reversible dissociation of the B873 light-harvesting complex from *Rhodospirillum rubrum* G9+. *Biochemistry*, **27**, 1004–1014.
- Ghosh, R., Rosatzin, T. & Bachofen, R. (1988b). Subunit structure and reassembly of the light-harvesting complex from *Rhodospirillum rubrum* G9+. In *Photosynthetic Light Harvesting Systems* (Scheer, H. &

- Schneider, S., eds), pp. 93–102, Walter de Gruyter, Berlin.
- Ghosh, R., Kessi, J., Hauser, H., Werli, E. & Bachofen, R. (1990). Quarternary structure of the B875 light-harvesting complex from *Rhodospirillum rubrum* G9+. In *Molecular Biology of Membrane-bound Complexes in Phototrophic Bacteria* (Drews, G. & Dawes, E. A., eds), pp. 245–251, Plenum Press, New York.
- Ghosh, R., Ghosh-Eicher, S., DiBerardino, M. & Bachofen, R. (1994). Protein phosphorylation in *Rhodospirillum rubrum*: purification and characterization of a water-soluble B873 protein kinase and a new component of the B873 complex, Ω , which can be phosphorylated. *Biochim. Biophys. Acta*, **1184**, 28–36.
- Goodhew, C. F., Brown, K. R. & Pettigrew, G. W. (1986). Haem staining in gels, a useful tool in the study of bacterial *c*-type cytochromes. *Biochim. Biophys. Acta*, **852**, 288–294.
- Harauz, G., Boekema, E. & van Heel, M. (1988). Statistical image analysis of electron micrographs of ribosomal subunits. *Methods Enzymol.* **164**, 35–49.
- Henderson, R., Baldwin, J. M., Downing, K. H., Lepault, J. & Zemlin, F. (1986). Structure of purple membrane from *Halobacterium halobium*: recording, measurement and evaluation of electron micrographs at 3.5 Å resolution. *Ultramicroscopy*, **19**, 147–178.
- Henderson, R., Baldwin, J. M., Ceska, T. A., Zemlin, F., Beckmann, E. & Downing, K. H. (1990). Model for the structure of *Bacteriorhodopsin* based on high-resolution electron cryo-microscopy. *J. Mol. Biol.* **213**, 899–929.
- Joliot, P., Vermeglio, A. & Joliot, A. (1990). Electron transfer between primary and secondary donors in *Rhodospirillum rubrum*: evidence for a dimeric association of reaction centers. *Biochemistry*, **29**, 4031–4037.
- Karrasch, S., Bullough, P. A. & Ghosh, R. (1995). The 8.5 Å projection map of the light-harvesting complex I from *Rhodospirillum rubrum* reveals a ring composed of 16 subunits. *EMBO J.* **14**, 631–638.
- Kessi, J., Poiree, J.-C., Wehrli, E., Bachofen, R., Semenza, G. & Hauser, H. (1994). Short-chain phosphatidylcholines as superior detergents in solubilizing membrane proteins and preserving biological activity. *Biochemistry*, **33**, 10825–10836.
- Kessi, J., Ghosh, R. & Bachofen, R. (1995). Purification of the LH-RC complex of *Rhodospirillum rubrum* by solubilisation of chromatophores with a short-chain lecithin. *Photosynth. Res.* **46**, 353–362.
- Koepke, J., Hu, X., Münke, C., Schulten, K. & Michel, H. (1996). The crystal structure of the light-harvesting complex II (B800-B850) from *Rhodospirillum rubrum*. *Structure*, **4**, 581–597.
- Laemmli, U. K. (1970). Cleavage of structural proteins during the assembly of the head of bacteriophage T4. *Nature*, **227**, 680–685.
- McDermott, G., Prince, S. M., Freer, A. A., Hawthornthwaite-Lawless, A. M., Papiz, M. Z., Codgell, R. J. & Isaacs, N. W. (1995). Crystal structure of an integral membrane light-harvesting complex from photosynthetic bacteria. *Nature*, **374**, 517–521.
- Miller, J. F., Hinchigeri, S. B., Parkes, Loach P. S., Callahan, P. M., Sprinkle, J. R., Riccobono, J. R. & Loach, P. A. (1987). Isolation and characterization of a subunit form, of the light-harvesting complex of *Rhodospirillum rubrum*. *Biochemistry*, **26**, 5055–5062.
- Miller, K. R. (1982). Three-dimensional structure of a photosynthetic membrane. *Nature*, **300**, 53–55.
- Penczek, P., Radermacher, M. & Frank, J. (1992). Three-dimensional reconstruction of single particles embedded in ice. *Ultramicroscopy*, **40**, 33–53.
- Peterson, G. L. (1977). A simplification of the protein assay method of Lowry *et al.* which is more generally applicable. *Anal. Biochem.* **83**, 346–356.
- Radermacher, M. (1988). Three-dimensional reconstruction of single particles from random and non-random tilt series. *J. Electron Microsc. Tech.* **9**, 359–394.
- Saegesser, R., Ghosh, R. & Bachofen, R. (1992). Stability of broad host range cloning vectors in phototrophic bacterium *Rhodospirillum rubrum*. *FEMS Microbiol. Letters*, **95**, 7–12.
- Saxton, W. O. (1996). Semper – distortion compensation, selective averaging, 3-D reconstruction, and transfer-function correction in a highly programmable system. *J. Struct. Biol.* **116**, 230–236.
- Saxton, W. O., Pitt, T. J. & Horner, M. (1979). Digital image processing: the Semper system. *Ultramicroscopy*, **4**, 343–354.
- Sistrom, W. R. (1977). Transfer of chromosomal genes mediated by plasmid R68.45 in *Rhodospseudomonas sphaeroides*. *J. Bacteriol.* **131**, 526–533.
- Thomas, P. E., Ryan, D. & Levin, W. (1976). An improved staining procedure for the detection of the peroxidase activity of cytochrome P-450 on sodium dodecyl sulfate polyacrylamide gels. *Anal. Biochem.* **75**, 168–176.
- Van Heel, M. (1984). Multivariate statistical classification of noisy images (randomly oriented biological macromolecules). *Ultramicroscopy*, **13**, 165–184.
- Walz, T. & Ghosh, R. (1997). Two-dimensional crystallization of the light-harvesting I-reaction centre photounit from *Rhodospirillum rubrum*. *J. Mol. Biol.* **265**, 107–111.
- Walz, T., Smith, B. L., Agre, P. & Engel, A. (1994). The three-dimensional structure of human erythrocyte aquaporin CHIP. *EMBO J.* **13**, 2985–2993.
- Wiggli, M., Cornacchia, L., Saegesser, R., Bachofen, R. & Ghosh, R. (1996). Characterisation of *Rhodospirillum rubrum* ST2. A new Tn5-induced carotenoid-less mutant for functional studies. *Microbiol. Res.* **151**, 1–5.
- Zuber, H. (1985). Structure of antenna polypeptides. In *Antennas and Reaction Centers of Photosynthetic Bacteria* (Michel-Beyerle, M. E., ed.), pp. 2–14, Springer-Verlag, Berlin.

Edited by R. Huber

(Received 18 November 1997; received in revised form 2 June 1998; accepted 2 June 1998)